

A physical model for strain accumulation in the San Francisco Bay region: Stress evolution since 1838

Fred Pollitz, William H. Bakun, and Marleen Nyst

U.S. Geological Survey, Menlo Park, California, USA

Received 29 January 2004; revised 4 May 2004; accepted 21 June 2004; published 30 November 2004.

[1] Understanding of the behavior of plate boundary zones has progressed to the point where reasonably comprehensive physical models can predict their evolution. The San Andreas fault system in the San Francisco Bay region (SFBR) is dominated by a few major faults whose behavior over about one earthquake cycle is fairly well understood. By combining the past history of large ruptures on SFBR faults with a recently proposed physical model of strain accumulation in the SFBR, we derive the evolution of regional stress from 1838 until the present. This effort depends on (1) an existing compilation of the source properties of historic and contemporary SFBR earthquakes based on documented shaking, geodetic data, and seismic data (Bakun, 1999) and (2) a few key parameters of a simple regional viscoelastic coupling model constrained by recent GPS data (Pollitz and Nyst, 2004). Although uncertainties abound in the location, magnitude, and fault geometries of historic ruptures and the physical model relies on gross simplifications, the resulting stress evolution model is sufficiently detailed to provide a useful window into the past stress history. In the framework of Coulomb failure stress, we find that virtually all $M \geq 5.8$ earthquakes prior to 1906 and $M \geq 5.5$ earthquakes after 1906 are consistent with stress triggering from previous earthquakes. These events systematically lie in zones of predicted stress concentration elevated 5–10 bars above the regional average. The SFBR is predicted to have emerged from the 1906 “shadow” in about 1980, consistent with the acceleration in regional seismicity at that time. The stress evolution model may be a reliable indicator of the most likely areas to experience $M \geq 5.5$ shocks in the future. **INDEX TERMS:** 1206 Geodesy and Gravity: Crustal movements—interplate (8155); 1236 Geodesy and Gravity: Rheology of the lithosphere and mantle (8160); 1243 Geodesy and Gravity: Space geodetic surveys; **KEYWORDS:** crustal deformation, plate boundary zones, viscoelastic relaxation, San Francisco Bay Region

Citation: Pollitz, F., W. H. Bakun, and M. Nyst (2004), A physical model for strain accumulation in the San Francisco Bay region: Stress evolution since 1838, *J. Geophys. Res.*, 109, B11408, doi:10.1029/2004JB003003.

1. Introduction

[2] The San Francisco Bay region (SFBR) is part of the San Andreas fault system in northern California (Figure 1), which accommodates a total of approximately 38 mm/yr right-lateral strike-slip motion across the multiple fault strands which traverse the region [Savage *et al.*, 1998; Argus and Gordon, 2001; Murray and Segall, 2001; Prescott *et al.*, 2001]. Historical seismicity in the SFBR exhibits striking patterns that have attracted considerable attention in recent years. The region has experienced several large earthquakes since 1769 [Ellsworth, 1990], and the catalog of SFBR earthquakes is likely complete for moment magnitude $M \geq 5.5$ since 1850 [Bakun, 1999]. As documented by Bakun [1999], the distribution of earthquakes since 1836 reveals that (1) the rate of $M \geq 6.5$ earthquakes since 1836 is approximately one every 30 years, (2) the production rate of $M \geq 5.5$ earthquakes in the 56 years prior

to the 1906 San Francisco earthquake was much higher than in the 70 years following it but the 1850–1906 moment release rate is about the same as that since 1977, and (3) large earthquakes have occurred not only on the dominant fault strand (San Andreas fault) but also on several subparallel fault strands.

[3] The moment release rate across the region, most of which is due to $M \geq 6.5$ earthquakes, is consistent with the buildup of strain that would be expected since 1836 given the ~ 38 mm/yr Pacific-Sierra Nevada/Great Valley (SNGV) relative plate motion. The contrast in seismicity rate during the period prior to the 1906 earthquake versus the period following it has been interpreted to be the result of the static Coulomb stress change imparted by the 1906 earthquake, which reduced much of the accumulated tectonic stress and cast the region into a “stress shadow” [Jaume and Sykes, 1996; Harris and Simpson, 1998]. Smaller shadows were cast by other large historic events such as the 1838 SF Peninsula and 1868 Hayward fault earthquakes [Jaume and Sykes, 1996], though their inhibiting effects on regional seismicity were only about 10–15 years. The occurrence of

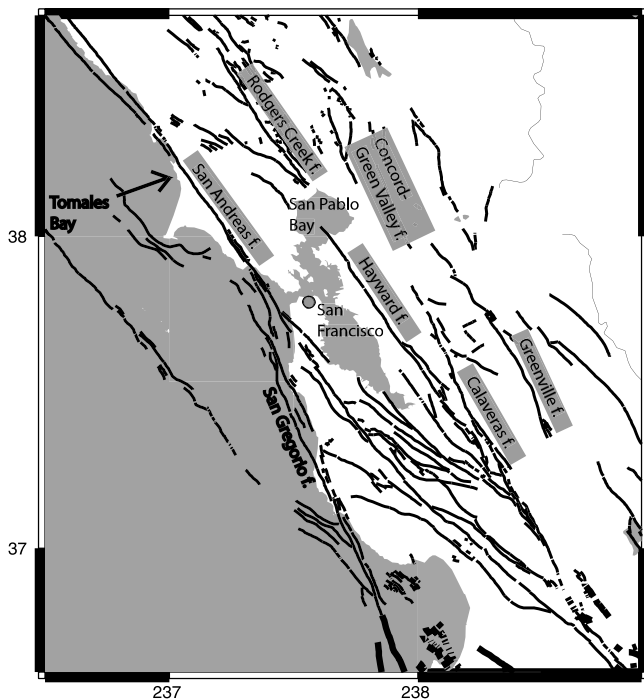


Figure 1. Map of San Francisco Bay region indicating major faults.

large earthquakes on faults other than the San Andreas fault, e.g., the Rodgers Creek, Hayward, and Calaveras faults, is recognized not only in the historical record but also in the paleoseismic record [Kelson *et al.*, 1992; Schwartz *et al.*, 1998; Lienkaemper *et al.*, 2002]. Analysis of geodetic data indicates that the San Andreas fault accommodates approximately 60% of the strain buildup that is eventually released in earthquakes, with 40% accommodated by other faults [Savage *et al.*, 1999; Murray and Segall, 2001]. Since the strike of the San Andreas fault in the SFBR is about 10 counterclockwise of the expected local Pacific-SNGV plate velocity vector [Argus and Gordon, 2001], the other faults help relieve the consequent buildup of fault-parallel plus fault-normal convergence by accommodating primarily strike-slip motion on fault strands parallel to the Pacific-SNGV velocity vector.

[4] The pattern of earthquake occurrence in the SFBR has more subtle details than just the 1906 static stress shadow effect documented to have inhibited 20th century seismicity. For example, Jaume and Sykes [1996] suggested that the acceleration in seismicity in the region from 1979 to 1989 is likely (at least in part) due to the erosion of the 1906 stress shadow by steady tectonic strain accumulation since 1906. Simpson and Reasenberg [1994] analyzed the static Coulomb stress changes imparted by the 1989 Loma Prieta earthquake. They found that static stress changes both encouraged and inhibited subsequent earthquake activity on neighboring faults. This finding was verified and analyzed in greater detail by Parsons *et al.* [1999]. Simpson and Reasenberg [1994], Galehouse [1997], and Lienkaemper *et al.* [1997] also established that the creeping parts of the San Andreas fault (SAF) system responded with an acceleration/deceleration in a manner consistent with the stress-

triggered local seismicity rate changes. Harris and Simpson [1998] suggested that the occurrence of an earthquake in 1911 on the Calaveras fault, well within the 1906 stress shadow, could be explained by rate- and state-dependent friction effects.

[5] The above studies have addressed some aspects of the historical record and interpreted them with the static stress change from a few large historic earthquakes and rate and state friction effects, but several intrinsic features of the observational record remain unexplained: (1) The rationalization of all $M > \sim 6$ earthquakes since about 1838 in terms of candidate physical mechanisms has not been pursued, (2) other physical processes, particularly viscoelastic relaxation of the lower crust and upper mantle following large earthquakes [Thatcher, 1983] has received, with few exceptions [Kenner and Segall, 1999; Parsons, 2002], little attention in the context of SFBR seismicity patterns, and (3) a very specific form of background Pacific-SNGV tectonic loading has been usually employed, namely, that in which faults are loaded by steady creep below a certain locking depth.

[6] Both Kenner and Segall [1999] and Parsons [2002] employed a finite element model that included loading of the SAF system through shear transmitted across the Pacific-SNGV plate boundary zone, as well as viscoelastic relaxation effects of the 1906 earthquake. Kenner and Segall [1999] examined candidate two-dimensional viscoelastic models of the lower crust constrained by strain measurements conducted since 1906, and they implemented the 1906 rupture in a two-dimensional geometry (i.e., infinitely long fault). Parsons [2002] implemented SFBR faults as three-dimensional (3-D) fault surfaces and employed and validated a temperature-derived, one-dimensional viscosity structure using recently collected GPS data. His model was further validated by matching long-term slip rates of SFBR faults with appropriate choices of the coefficient of friction governing the behavior of each fault in the system. In order to predict post-1906 stress evolution, post-1906 relaxation effects were evaluated in the presence of continually slipping faults controlled by their respective coefficients of friction. Regional faults were locked in the upper 12.5 km but permitted to slip at greater depth.

[7] In this paper we implement faults as 3-D planar dislocation surfaces which occupy the elastic portion of a vertically stratified viscoelastic medium (i.e., elastic upper crust overlying a stratified viscoelastic plastosphere). Fault surfaces accommodate shear dislocations at the time of an earthquake, and during the period after an earthquake, the plastosphere relaxes with the faults locked until the next earthquake. We compile the relevant historical earthquakes that have affected the SFBR since 1838. Using these earthquakes as sources of deformation in the framework of Coulomb failure theory, we analyze the occurrence of moderate to large earthquakes since 1838 to test whether they are consistent with stress triggering from preceding earthquakes. This analysis depends on the determination of time-dependent stress on a representative regional viscoelastic model that is driven by a combination of background tectonic loading and relaxation of the plastosphere. Assumption of uniform stress levels in the region prior to 1838 is implicit. One can imagine a pathological state of stress before 1838 that would nullify the chief characteristics of the stress fields to be presented here. It is beyond

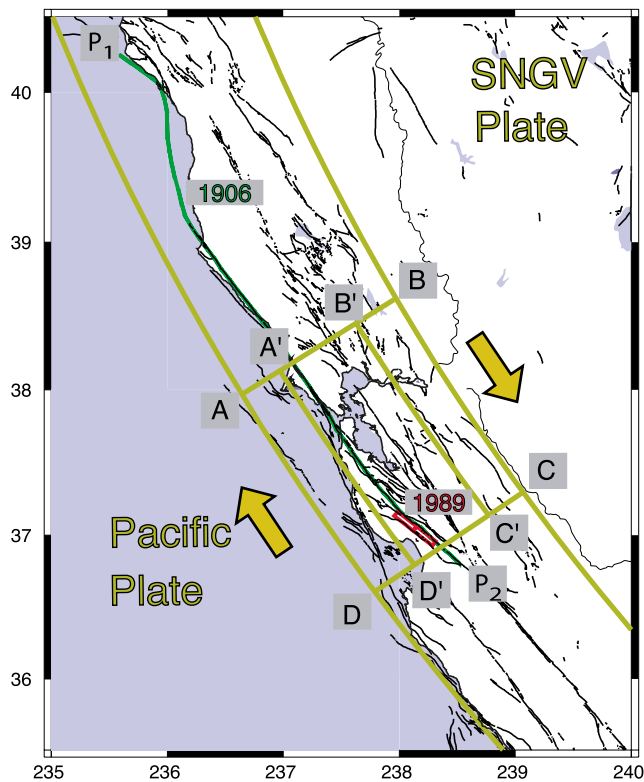


Figure 2. SNGV-Pacific plate boundary zone delineated by two small circles about a pole Ω_1 located at 46°N, 100°W. The spherical rectangles defined by points A–B–C–D and A’–B’–C’–D’ indicate that portion of the plate boundary zone in the SFBR spanning its entire width and its central part, respectively. P₁ and P₂ are the endpoints of the 1906 rupture (slip distribution given in Figure 10).

the scope of this paper to address the effect that possible pre-1838 perturbations would have had on subsequent stress evolution, except to note that the magnitude of such perturbations might be expected to be small based on the absence of $M \geq 7$ earthquakes between 1776 and 1838 [Ellsworth, 1990] and smoothing of long-wavelength stress fluctuations that is theoretically expected to occur in the absence of large earthquakes [Ben-Zion et al., 2003].

[8] In section 2 we describe the elements of the physical model that are needed to estimate the regional stress evolution from the history of past earthquakes. In section 3 we present the regional stress evolution using a single measure, the accumulated change in the Coulomb failure function since 1838, followed in section 4 by a discussion of the correlation of the predicted stress pattern with the observed pattern of potentially triggered earthquakes. We find that virtually all moderate to large regional earthquakes since 1838 are located in areas that are loaded 5 to 10 bars above the regional average.

2. Ingredients of SFBR Active Deformation

2.1. Physical Model

[9] A complete description of the processes of tectonic loading, stress changes due to earthquakes, and subsequent relaxation of a 3-D viscoelastic Earth is presently a

very challenging task. Pollitz and Nyst [2004, hereafter PN04] proposed a useful approximate solution: a physical model for strain accumulation in which the SFBR is regarded as a uniform width plate boundary zone (Figure 2) with relatively thin, pliable lithosphere, surrounded by relatively nondeformable Pacific and SNGV lithosphere due to their greater lithospheric thickness. The plate boundary zone (PBZ) is assumed to have laterally homogeneous material properties. It consists of an upper elastic layer underlain by viscoelastic lower crust and upper mantle (Figure 3). The PBZ is loaded by predominantly horizontal shear transmitted by the Pacific-SNGV relative motion plus a minor amount of regional compression. This is expressed through constant velocity boundary conditions on the Pacific-PBZ and PBZ-SNGV edges. Sources of deformation include earthquakes, which occur episodically, associated postseismic relaxation, and steady fault creep. Earthquakes are implemented as dislocations on 3-D fault planes embedded in a vertically stratified (1-D) viscoelastic Earth model.

[10] Previous modeling of the regional stress evolution [Jaume and Sykes, 1996; Murray and Segall, 2001] has assumed that regional faults are loaded by deep slip beneath a “locking depth,” above which the faults are locked during the interseismic period. An alternative framework is provided by the viscoelastic coupling model [Savage and Prescott, 1978] in which an infinitely long strike-slip fault occupying an upper elastic layer slips periodically. The system evolves as the underlying ductile “plastosphere” relaxes following each slip event. Depending on the viscosity of the plastosphere, the stress evolution at a particular point may be approximately linear (large Maxwell relaxation time) or highly nonlinear (small Maxwell relaxation time). In the context of the viscoelastic coupling model, Savage et al. [1999] pointed out that the expedient of using a locking depth model of strain accumulation around a strike-slip fault is valid only if the mean recurrence interval of the fault is shorter than the Maxwell relaxation time of the plastosphere. When this condition is met, the average interseismic velocity during a cycle is well approximated by plastosphere relaxation from past earthquakes without the need to invoke steady slip beneath a locking depth. Viscoelastic coupling models are further attractive because they capture the variation in velocity during a cycle [Thatcher, 1983]. A variation of the viscoelastic coupling model allows

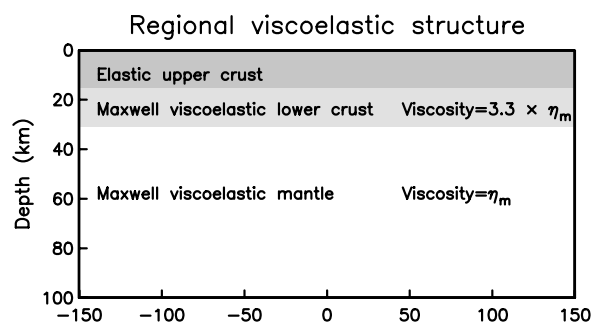


Figure 3. One-dimensional viscoelastic stratification of the SFBR assumed in this study, following model B of Pollitz et al. [1998].

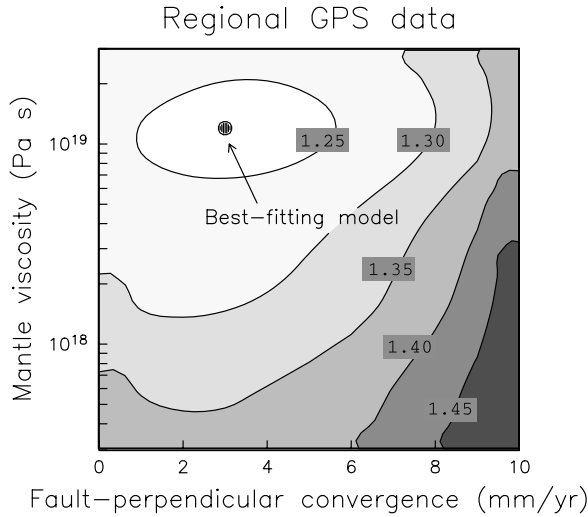


Figure 4. Results of grid search for η_m and v_2 to minimize reduced χ^2 for a GPS velocity field covering the time period 1994–2001 [Pollitz and Nyst, 2004]. The best fitting model is obtained at $\eta_m = 1.2 \times 10^{19}$ Pa s and $v_2 = 2.9$ mm/yr.

for the presence of a finite width shear zone that bounds a weak lithosphere-plastosphere system [Pollitz, 2001]. In the case of a two-dimensional strike-slip fault geometry, this model prescribes loading of the PBZ through horizontal forces transmitted at the edges of the PBZ, and it allows simultaneously for plastosphere relaxation following earthquakes and constant velocity boundary conditions at the PBZ edges. Except on specified creeping segments, faults are considered locked during interseismic intervals. In the finite fault geometries to be modeled here, we employ an exact solution for plastosphere relaxation following imposed earthquakes combined with an approximate matching of the boundary conditions at these edges.

[11] There is a strong contrast in material properties between the PBZ and the surrounding plates which have much thicker lithosphere. In principle, the equations of quasi-static equilibrium should be solved on this 3-D heterogeneous viscoelastic system subject to the background velocity conditions. PN04 found a solution which satisfies the equations of quasi-static equilibrium within the PBZ plus the corresponding boundary conditions to a high degree of accuracy; very small mismatches remain only at the boundaries that divide the Pacific plate from the PBZ and SNGV plate from the PBZ, and these are considered inconsequential since they are far from the central part of the PBZ where velocities and stresses are to be evaluated. The approximate solution utilizes a superposition of a known viscoelastic solution [Pollitz, 1997] and static solution [Pollitz, 1996] for deformation from prescribed dislocation sources on a laterally homogeneous model, plus additional elementary solutions to construct a velocity field that deviates from the exact solution only in small time-dependent mismatches in the boundary conditions in the shear or contractile components. For a prescribed history of earthquakes this solution, which is described in detail in PN04, yields time-dependent velocity and stress fields within the PBZ, and it forms the basis for the modeling to be described.

[12] Briefly summarizing the method of PN04, the time-dependent velocity field $\mathbf{v}(\mathbf{r}, t)$ at points \mathbf{r} within the PBZ has the form

$$\mathbf{v}(\mathbf{r}, t) = \sum_i \mathbf{v}_{ps}^{(i)}(\mathbf{r}, t) + \sum_j \mathbf{v}_{cr}^{(j)}(\mathbf{r}) + v_1(t) \left(\frac{\delta}{W} \right) \hat{\mathbf{r}} \times \frac{\hat{\Omega}_1}{|\hat{\mathbf{r}} \times \hat{\Omega}_1|} + v_2 \left(\frac{\delta}{W} \right) \hat{\mathbf{r}} \times \hat{\Omega}_2 + \hat{\mathbf{r}} \times \boldsymbol{\Omega}(t) \quad (1)$$

where δ and W represent the distance of the observation point from the SNGV plate boundary and the width of the PBZ, respectively. This expresses the total velocity field as a sum of five components: (1) $\sum_i \mathbf{v}_{ps}^{(i)}(\mathbf{r}, t)$, the combined postseismic relaxation from past events calculated on the laterally homogeneous model, (2) $\sum_j \mathbf{v}_{cr}^{(j)}(\mathbf{r})$, the sum of steady creep effects from a collection of creeping faults, (3) $v_1(t) (\delta/W) \hat{\mathbf{r}} \times \hat{\Omega}_1 / |\hat{\mathbf{r}} \times \hat{\Omega}_1|$, simple shear within the PBZ (arbitrary time dependence) with net velocity v_1 accommodated across the PBZ, (4) $v_2 (\delta/W) \hat{\mathbf{r}} \times \hat{\Omega}_2$, uniform uniaxial compression along a direction perpendicular to the local trend of the plate boundary, with a net convergence rate of v_2 (assumed constant with time) accommodated across the PBZ, and (5) rigid rotation about an Euler pole $\boldsymbol{\Omega}$ (arbitrary time dependence).

[13] PN04 used recent GPS measurements from 1994 to 2001 to calibrate this model. The poles $\hat{\Omega}_1$ and $\hat{\Omega}_2$ were specified a priori: $\hat{\Omega}_1$ lies near the SNGV-Pacific Euler pole, and $\hat{\Omega}_2$ is defined to lie 90° away from the PBZ along a great circle that passes through the PBZ and is locally tangent to it (PN04). The GPS measurements serve to simultaneously determine the viscoelastic stratification (i.e., value of η_m) and the net PBZ-perpendicular velocity v_2 (assumed independent of time). Then for a given past history of earthquakes PN04 solved for average $v_1(t)$ (for the 1994 to 2001 time period) and average $\boldsymbol{\Omega}(t)$ (three components) which best satisfied constant velocity boundary conditions on the Pacific and SNGV plate boundary edges in a least squares sense. More precisely, for the 1994–2001 time period both the mantle viscosity value η_m and the net PBZ-perpendicular velocity v_2 were determined in a grid search simultaneously with average $v_1(t)$ and $\boldsymbol{\Omega}(t)$. The minimum misfit region obtained in the grid search corresponds to (Figure 4) $\eta_m = 1.2 + 0.6 / -0.4 \times 10^{19}$ Pa s and $v_2 = 3 \pm 1.5$ mm/yr (quoted errors are one standard deviation). We have carried this procedure further by fixing η_m , $\hat{\Omega}_1$ and $\hat{\Omega}_2$, and v_2 at the values determined by PN04, then applying constant velocity boundary conditions within selected time intervals since an initial time (1838) to derive the required $v_1(t)$ and $\boldsymbol{\Omega}(t)$.

[14] The time-dependent displacement field $\mathbf{u}(\mathbf{r}, t)$ is obtained by integrating equation (1) with respect to time and including the elastic deformation fields resulting from coseismic effects of earthquakes. Let t_0 be the initiation time of the system and $\{t_i\}$ a set of occurrence times of the source earthquakes. Then

$$\mathbf{u}(\mathbf{r}, t) = \sum_i \mathbf{u}_i(\mathbf{r}) + \sum_i \int_{t_0}^t \mathbf{v}_{ps}^{(i)}(\mathbf{r}, t') dt' + (t - t_0) \cdot \sum_j \mathbf{v}_{cr}^{(j)}(\mathbf{r}) + \int_{t_0}^t v_1(t') dt' \left(\frac{\delta}{W} \right) \hat{\mathbf{r}} \times \frac{\hat{\Omega}_1}{|\hat{\mathbf{r}} \times \hat{\Omega}_1|} + v_2 (t - t_0) \left(\frac{\delta}{W} \right) \hat{\mathbf{r}} \times \hat{\Omega}_2 + \int_{t_0}^t \hat{\mathbf{r}} \times \boldsymbol{\Omega}(t') dt' \quad (2)$$

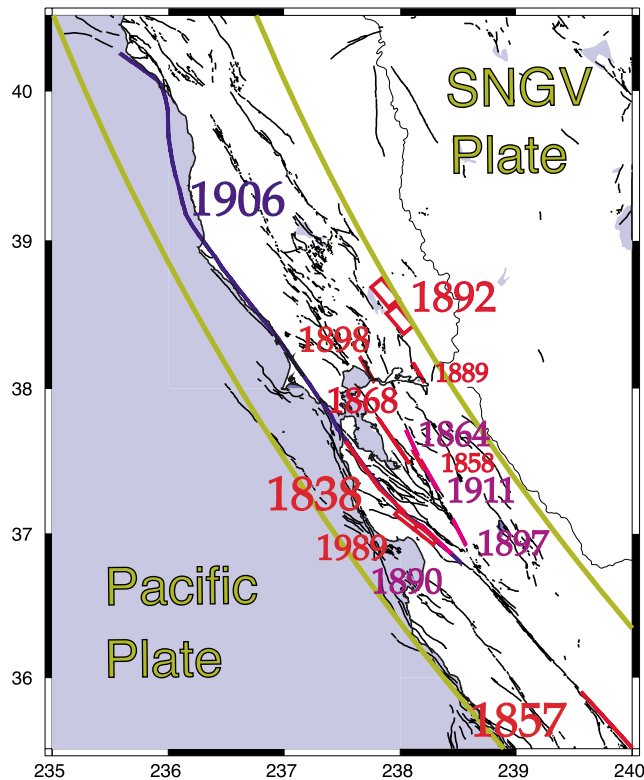


Figure 5. Source earthquakes used in this study. This includes all $M \geq 6.2$ earthquakes listed in Table 2 of *Bakun* [1999], except for the omission of the 8 October 1865 $M = 6.5$ earthquake and the inclusion of two smaller historical events on the Calaveras fault near one another which together define an equivalent larger event: the 5 March 1864 $M = 5.9$ and 21 May 1864 $M = 5.6$ earthquakes. (Different colors for fault segments are used to help distinguish among them.)

Here \mathbf{u}_i represents the elastic displacement field resulting from the i th source earthquake. Equation (2) allows us to obtain a time-dependent stress tensor $\sigma(\mathbf{r}, t)$ that will be utilized in analysis of fault interaction in the SFBR in section 3.

2.2. Sources of Deformation

[15] Fifteen earthquakes of magnitude $M \geq 6.2$ occurring from 1838 to 1989 (Figure 5) are used as sources of deformation in this study. Corresponding source parameters are listed in Table 1. The locations and magnitudes of historical events (prior to about 1943 when routine determination of magnitude at Berkeley started) are generally uncertain. A typical uncertainty in epicenter location and magnitude are ± 10 km and ± 0.2 magnitude units, respectively [*Bakun*, 1999]. For larger events ($M > \sim 6.7$), not only location but fault dimensions become important, and there is generally little guidance to the precise locations of the slip planes involved with the event. For most events we follow *Bakun* [1998, 1999] in assigning source parameters (fault length, dip, upper and lower edge depth, slip) to the events. Two smaller events which occurred in close proximity to one another on the Calaveras fault, the March, 1864 $M = 6.0$ and May, 1864 $M = 5.8$ events, are included as they could be grouped into a single larger event. For the 31 March 1898 $M = 6.3$ Mare Island event we have chosen a location at the mouth of the Napa River based on documented damage to Mare Island; this is similar to scenario B of *Bakun* [1998]. For the June 1838 Peninsula earthquake, which has a range of possible magnitudes from 6.8 to 7.5 [*Topozada and Borchardt*, 1998; *Bakun*, 1999], we are guided by three pieces of evidence: (1) the earthquake did not apparently rupture north of the Golden Gate [*Topozada and Borchardt*, 1998], (2) shaking was strong in both Oakland (MMI VII) and Monterey Bay (MMI VI 1/2), and (3) no surface slip has been detected at Grizzly Flat on the San Andreas fault south of Woodside [*Schwartz et al.*, 1998]. On the basis of these considerations we choose a fault length of 75 km extending from the San Francisco peninsula southward to just north of Grizzly Flat (Figure 5), corresponding to a $M = 7.1$ event. We find that the chosen fault dimensions yield long-lived stress patterns that lead, in particular, to a stress maximum near the future rupture zones of large earthquakes in the southern Santa Cruz mountains (in 1865 and 1989; section 3.2). If a longer fault length had been chosen (extending farther toward the southeast), we find that the resulting stress patterns would be inconsistent with the occurrences of the 1865 and 1989 earthquakes.

Table 1. Large Historical Earthquakes

Earthquake	Fault Type	$M_0, 10^{20}$ N m	Magnitude	Reference
June 1838	strike-slip	0.75	7.2	<i>Tuttle and Sykes</i> [1992]
		0.18	6.8	<i>Bakun</i> [1999]
		2.00	7.5	<i>Topozada and Borchardt</i> [1998]
January 1857	strike-slip	10.00	8.0	<i>Sieh</i> [1978]
November 1858	strike-slip	0.03	6.3	<i>Bakun</i> [1999]
March 1864	strike-slip	0.01	6.0	<i>Topozada et al.</i> [2002]
May 1864	strike-slip	0.006	5.8	<i>Topozada et al.</i> [2002]
October 1868	strike-slip	0.30	7.0	<i>Yu and Segall</i> [1996]
May 1889	strike-slip	0.03	6.3	<i>Bakun</i> [1999]
April 1890	strike-slip	0.03	6.3	<i>Bakun</i> [1999]
April 1892	two thrust events	0.08	6.5	<i>O'Connell et al.</i> [2001]
		0.03	6.3	
June 1897	strike-slip	0.03	6.3	<i>Bakun</i> [1999]
March 1898	strike-slip	0.06	6.5	<i>Topozada et al.</i> [2002]
		0.03	6.3	<i>Bakun</i> [1999]
		0.03	6.3	<i>Bakun</i> [1999]
April 1906	strike-slip	8.20	7.9	<i>Thatcher et al.</i> [1997]
July 1911	strike-slip	0.02	6.2	<i>Bakun</i> [1999]
October 1989	oblique-slip	0.26	6.9	<i>Marshall et al.</i> [1991]

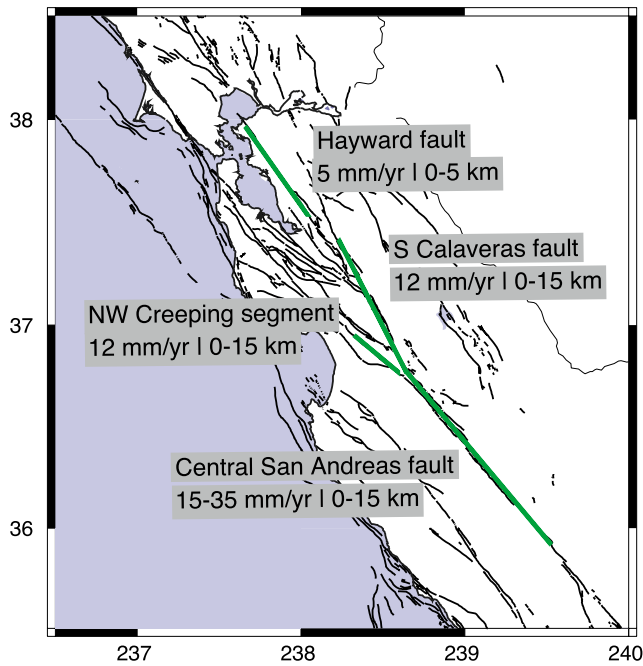


Figure 6. Surface traces of creeping faults. The depth range and value of steady slip are assigned as indicated.

This is in harmony with the independent finding of *Fumal et al.* [2003] that the 1838 earthquake is not recognized in the paleoseismic record of the San Andreas fault near Pajaro Gap in the southern Santa Cruz mountains.

[16] Remaining larger historical earthquakes have generally better constrained source properties because (beginning with the 1868 Hayward fault event) they are constrained by geodetic data. For the 1868 earthquake we use the fault model of *Yu and Segall* [1996], for the 1906 San Francisco we use the distributed slip model of *Thatcher et al.* [1997], and for the 1989 Loma Prieta earthquake we use the two-plane fault model of *Marshall et al.* [1991]. The 1892 Winters-Vacaville earthquakes (two $M \sim 6.4$ earthquakes) are not constrained by geodetic data, but both the magnitude and approximate fault geometry [*O'Connell et al.*, 2001] are known well enough to make them useful source faults. For smaller earthquakes the reports of shaking improved greatly after about 1850 as the population increased owing to the gold rush, leading to better inferences of epicenter locations. The key unknown is the depth extent of faulting which controls to a large extent not only the coseismic deformation field but also the nature of postseismic relaxation, which is very sensitive to the distance between the base of the fault and the top of the ductile zone (i.e., top of the lower crust). We assume that large events penetrate the entire elastic layer from 0 to 15 km depth, which is approximately the seismogenic layer thickness [*Hole et al.*, 2000], but smaller events rupture a more limited depth extent according to their moment [e.g., *Bakun*, 1998, 1999]. A second source of deformation is steady creep on faults. We describe the creeping portions of SFBR faults with the fault segments shown in Figure 6. We specify a priori the depth range and rate of slip on these faults as follows: Hayward fault, 0–5 km, 5 mm/yr based on *Savage and Lisowski* [1993]; central San Andreas fault, 0–15 km, variable slip rate

15–35 mm/yr [*Rymer et al.*, 1984]; NW creeping segment, 0–15 km, 12 mm/yr; South Calaveras fault, 0–15 km, 12 mm/yr [*Oppenheimer et al.*, 1990]. The velocity field produced by steady creep of these segments is evaluated in the fluid limit of the viscoelastic model in a spherical geometry using the method of *Pollitz* [1996].

[17] Specification of the above sources of deformation in combination with the viscoelastic structure completely determines the deformation field as described in section 2.1. After determining time-dependent $v_1(t)$ and $\Omega(t)$ we may evaluate how well the boundary conditions on the Pacific and SNGV plate edges have been satisfied. Figure 7 shows the model velocity field evaluated on both the Pacific-PBZ and SNGV-PBZ edges, resolved into those components parallel to and perpendicular to the relative plate motion direction. Except for the area north of San Francisco during the first few decades following 1906 (where relaxation effects were very strong because of the large slip in the north Bay), all velocities within the SFBR are within

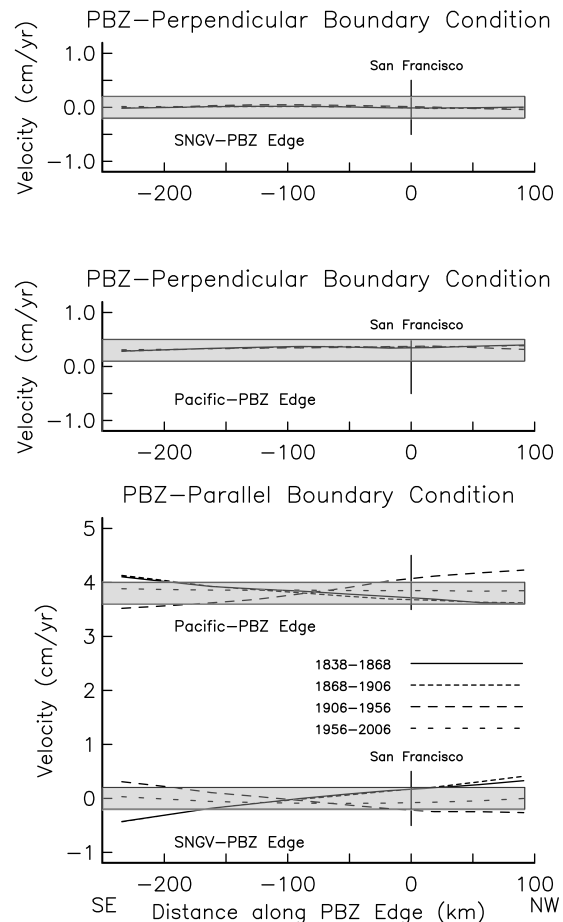


Figure 7. Model velocity field evaluated on the Pacific-PBZ and SNGV-PBZ edges (shown in Figure 2) as a function of distance from San Francisco (on the Pacific-PBZ edge). The velocity field is resolved into its components parallel to and perpendicular to the local plate boundary azimuth. Grey boxes delineate those velocities that are within 2 mm/yr of the exact boundary conditions: 38 mm/yr PBZ-parallel motion and 3 mm/yr PBZ-perpendicular motion on the Pacific-PBZ edge.

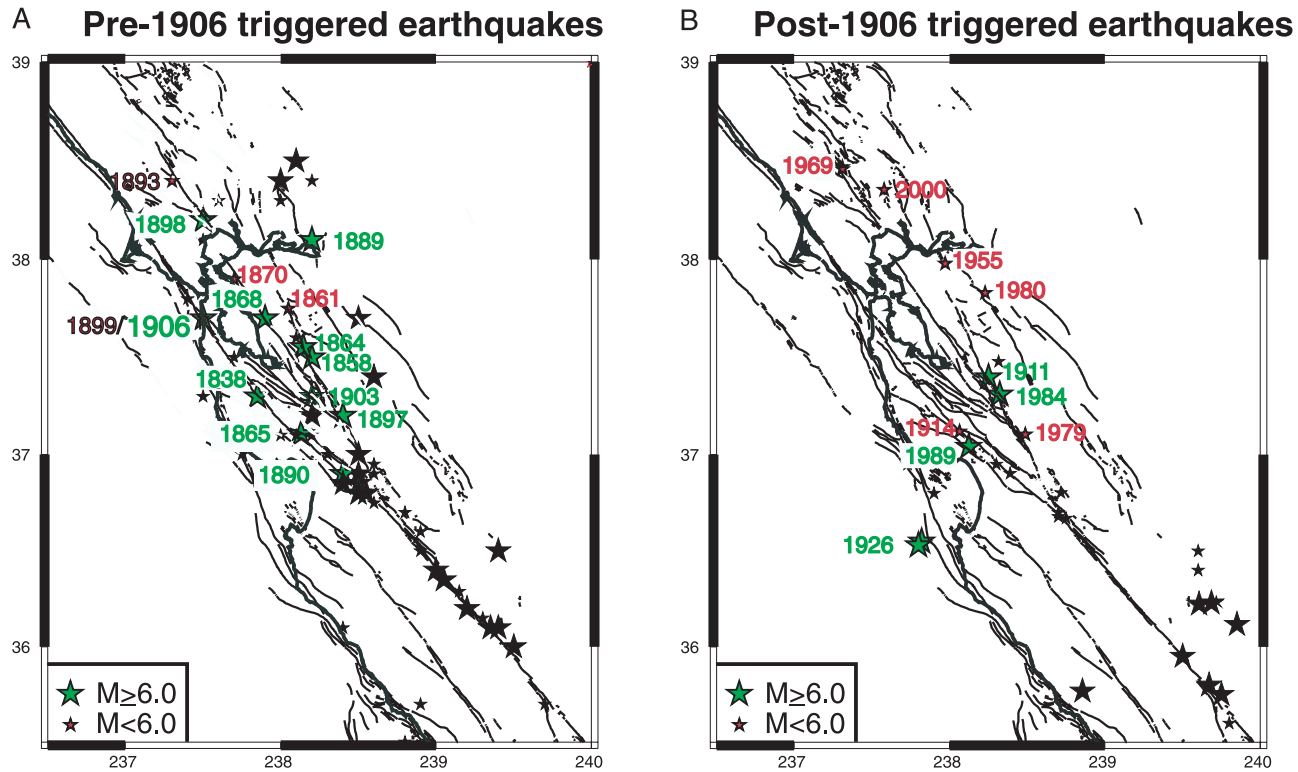


Figure 8. (a) Pre-1906 and (b) post-1906 potentially triggered earthquakes. Locations and magnitudes are from *Bakun* [1998, 1999] and *Topozada and Branum* [2002]. Black stars show other earthquakes listed in the Topozada and Branum catalog which we do not consider. The great majority of these are located on the creeping portions of the Calaveras and San Andreas faults south of 37°N. The triggered earthquakes shown in Figure 8b include all pre-1906 earthquakes of magnitude $M \geq 5.8$ and post-1906 earthquakes of magnitude $M \geq 5.5$, with the exception of the $M_{5.2}$ Yountville earthquake. Note that the 1865 earthquake is placed in accordance with scenario B of *Bakun* [1998].

2 mm/yr of the exact boundary conditions (38 mm/yr PBZ-parallel motion and 3 mm/yr fault-perpendicular motion on the Pacific-PBZ edge; zero motion on the SNGV-PBZ edge).

3. Stress Evolution

3.1. Coulomb Failure Stress

[18] We define the time-dependent coulomb failure function [*Reasenberg and Simpson*, 1992; *King et al.*, 1994; *Stein*, 1999], representing the total change in Coulomb failure stress accumulated since an initial time:

$$\sigma_f(\mathbf{r}, t) = \tau(\mathbf{r}, t) + \mu' \sigma_n(\mathbf{r}, t) \quad (3)$$

where τ and σ_n represent the shear and normal stress (positive tensile) resolved on a given secondary fault plane with prescribed slip vector, respectively, and μ' is the effective coefficient of friction. Both τ and σ_n are determined from the displacement field (equation (2)) and the secondary fault geometry. Since σ_f here represents accumulated stresses since 1838, we take $t_0 = 1838$ in equation (2). We fix the geometry of secondary faults to be vertical N34°W trending planes that undergo right-lateral slip. Although the secondary fault trends in the study area vary from N20°W to N42°W, the choice of N34°W is found to adequately capture the resulting stress patterns. The

coefficient of friction may vary from 0 to 0.8 [*Stein*, 1999], and for concreteness we choose the value $\mu' = 0.4$.

3.2. Potentially Triggered Earthquakes

[19] Figure 8 displays potentially triggered earthquakes considered in this study. These include all earthquakes of magnitude $M \geq 5.8$ prior to 1906 and $M \geq 5.5$ subsequent to 1906. These cutoffs were chosen to enable selection of pre-1906 earthquakes with reasonably well-understood ruptures (many $M \sim 5.5$ pre-1906 events listed by *Bakun* [1999] have poorly determined locations), and at the same time capture significant post-1906 earthquakes. Most of the $M \geq 5.5$ post-1906 earthquakes have occurred during the instrumental recording period, and most have occurred on fault segments that are considered fully locked rather than creeping (two exceptions are the 1979 Coyote Lake and 1894 Morgan Hill earthquakes). Many of the potentially triggered earthquakes are themselves source earthquakes. We have not included the 1892 Winters-Vacaville earthquakes, which are likely blind thrust events [*O'Connell et al.*, 2001] as triggered events because they are practically isolated events, very distant from the considered earlier events. For example, depending on dip of the 1892 ruptures, postseismic σ_f from the 1868 earthquake can be either positive or negative with magnitude ~ 0.05 bars. We have purposefully excluded events on the creeping sections of the central San Andreas and southernmost Calaveras faults

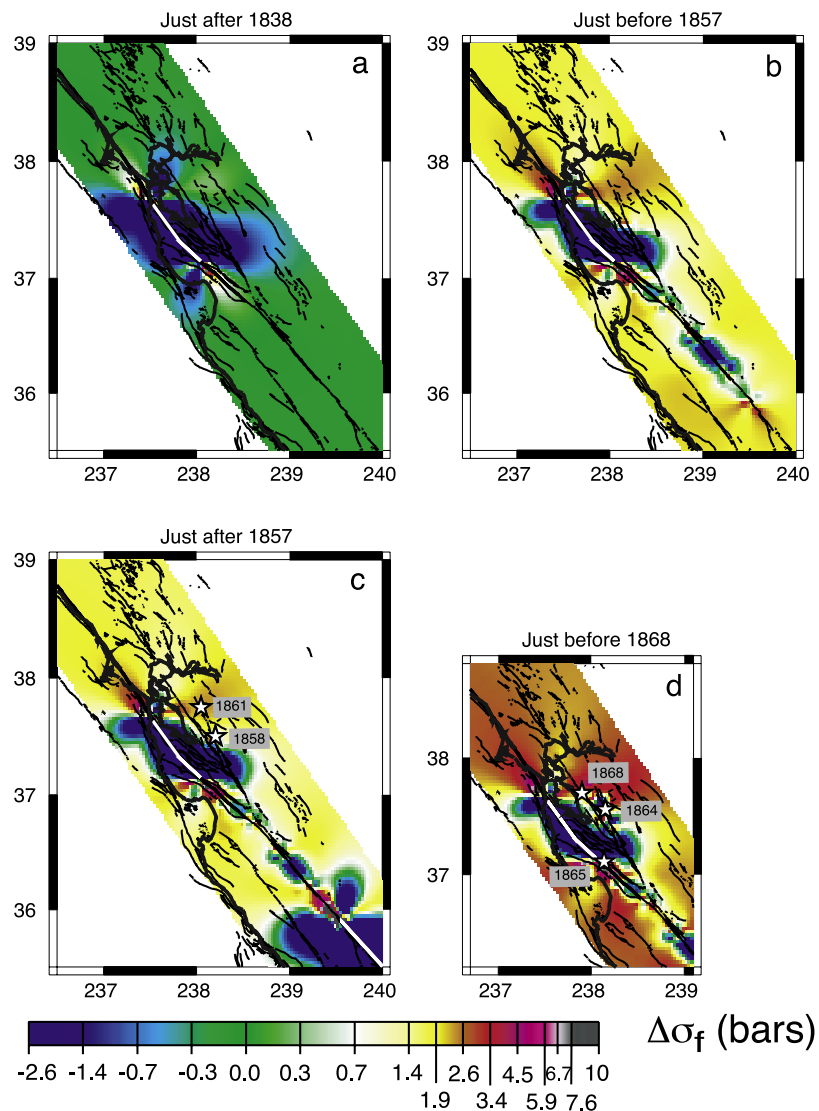


Figure 9. Evolution of σ_f (accumulated since 1838) at a depth of 8 km depicted in a series of snapshots. Superimposed are the epicenters of potentially triggered earthquakes that occurred close to the time of the given snapshot. White lines show the surface projections of fault planes associated with source fault planes that ruptured prior to the given time. Note a change of color scale between pre-1906 and post-1906 stress patterns. Contours associated with 1989 coseismic stress change are indicated with numerals in bars.

because of the elevated background seismicity rates on those segments. The remaining events are likely predominantly right-lateral strike-slip earthquakes on vertical or near-vertical faults trending from N20°W to N42°W.

3.3. Stress Evolution Since 1838

[20] The pattern of σ_f at a depth of 8 km at selected times is shown in Figures 9a–9q. The various subplots include the locations of potentially triggered earthquakes that occurred at approximately the time of the snapshot plus the source planes which contributed to modeled σ_f up to that time. One may systematically track the evolution of stress starting with the 1838 earthquake. The σ_f pattern at time 1838⁺ (Figure 9a, where superscript plus indicates just after the 1838 earthquake) is the coseismic stress change associated with the earthquake. It contains the expected large negative σ_f (“shadow”) regions surrounding the fault, positive lobes

off the tips of the fault, and secondary positive and negative lobes adjacent to the fault tips reflecting the effect of the normal stress change (unclamping and clamping effects). The σ_f pattern in 1857⁻ (Figure 9b, where superscript minus indicates just before the 1857 earthquake) has evolved owing to the combined effects of tectonic loading, steady fault creep, and postseismic relaxation of the lower crust and upper mantle. These effects are nearly independent of one another but slightly coupled because each contributes to the relative velocity at the PBZ edges, so that the $v_1(t)$ term of equation (2) is coupled to the \mathbf{v}_{cr} and \mathbf{v}_{ps} terms. The loading effect imparts positive σ_f to the entire region, while the postseismic relaxation effect leads to increased σ_f near the fault but decreased σ_f more than ~ 15 km from the fault. At distances less than 20–30 km from the fault, the relaxation effect dominates because the shadow clearly grows outward. On the other hand, the combined effects

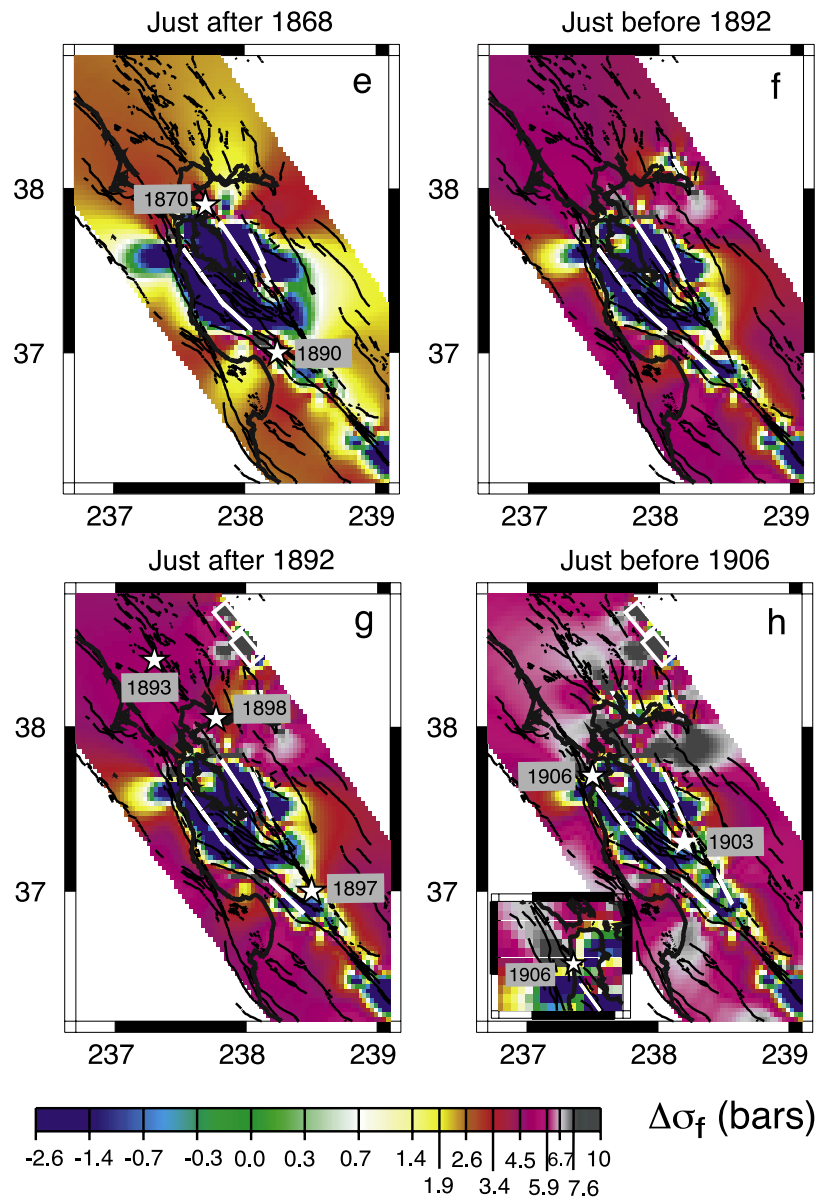


Figure 9. (continued)

of loading and relaxation tend to rapidly reload the neighborhood of the fault zone. The relatively rapid erosion of the shadow zone near the fault, where the shadow is initially the strongest, is a self-stabilizing property of this type of viscoelastic coupling model [Savage and Prescott, 1978; Pollitz, 2001].

[21] Continuing forward in time, one sees a slight difference in σ_f between 1857⁺ (Figure 9c) and 1857⁻ (Figure 9b) that is just the coseismic deformation field of the 1857 earthquake. Just after 1857, although the San Francisco Peninsula region lies in a deep shadow, much of the East Bay is in a zone of stress concentration. A few moderate earthquakes occurred around that time (1858, 1861, 1864) in this relatively high σ_f zone. At time 1868⁻ (Figure 9d) two larger earthquakes apparently nucleate in relatively high σ_f zones: the 1865 $M = 6.5$ and 1868 $M = 7.0$ events. The location of neither epicenter is certain. The 1865 event is particularly unclear since there was no ground rupture

associated with the event and shaking data alone allow a location either in the southern Santa Cruz Mountains (where we have placed it) or farther north near the Berrocal fault zone [Bakun, 1999]. Triangulation data analyzed by Yu and Segall [1996] suggest a thrust faulting mechanism on a NW-SE trending fault located somewhere between the southern Santa Cruz mountains and Berrocal fault zone in order to produce northeastward displacement of a triangulation station at Loma Prieta, hence our tentative choice of location. If it was indeed located on a thrust structure near the San Andreas fault and south of 37.1°N, then it would lie in a zone of elevated σ_f . Regarding the 1868 Hayward earthquake, the associated fault is unambiguously the Hayward fault based on observed surface rupture, and the extent of the fault involved in the rupture is constrained by geodetic data to be about a 52 km part of the southern Hayward fault [Yu and Segall, 1996]. The only rationale for placing the nucleation zone near the northern part of the

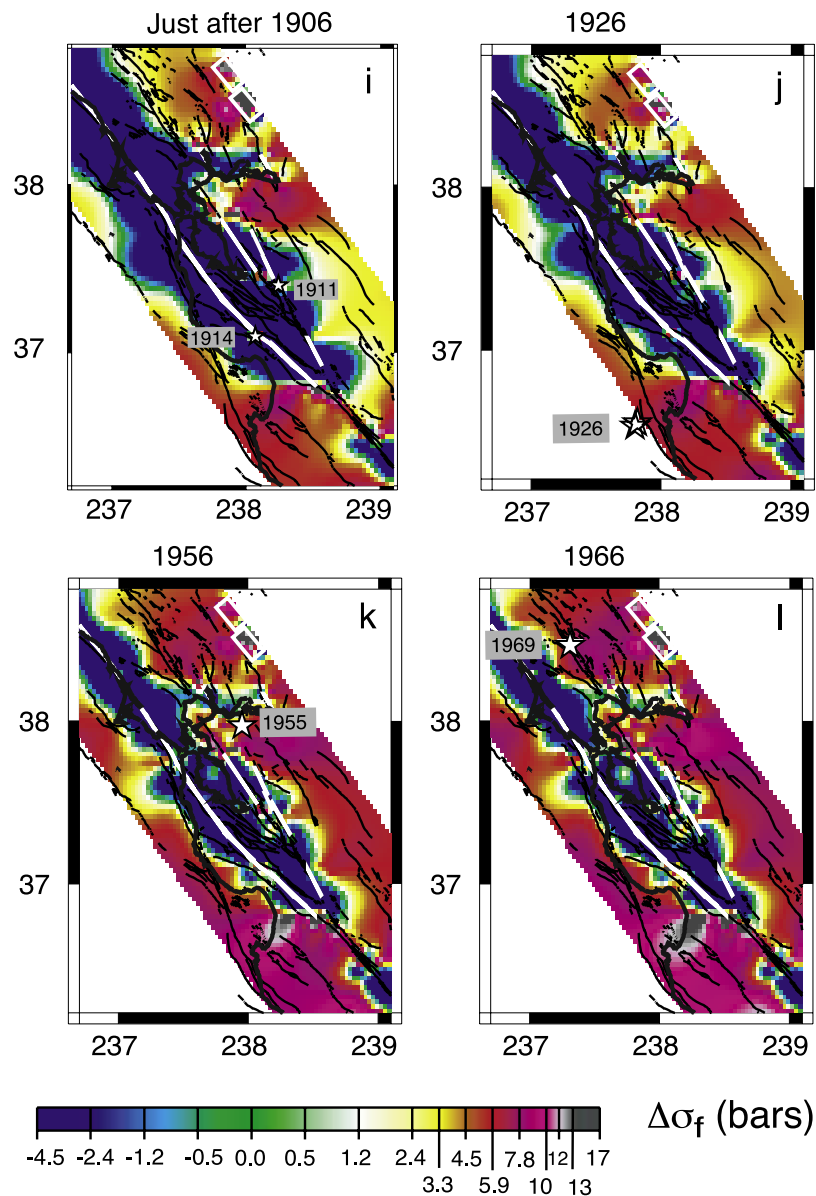


Figure 9. (continued)

rupture is that creep rates along the Hayward fault decrease toward the north, which have been interpreted by *Simpson et al.* [2001] as a shallowing of the locked zone toward the north. According to our model, the highest σ_f at the time of the 1868 earthquake was on the northern part of the impending rupture, so that an epicenter location there would be well correlated with relatively high σ_f . Given the uncertain locations of the nucleation points of the 1865 and 1868 ruptures, a positive correlation of the true location with modeled stress changes cannot be claimed, and the positive σ_f obtained for these two earthquakes neither supports nor contradicts the more robust correlations obtained for other 19th century events.

[22] After the 1868 earthquake (Figure 9e) a shadow zone enveloped the San Francisco Peninsula and most of the East Bay, but pockets of high σ_f remained in the south Bay, and the north Bay stress level simply continued to increase because of tectonic loading effects and the lack of stress release in the area. From 1870 up to the time of the 1906

earthquake (Figures 9e–9h), many earthquakes occurred in the south Bay and north Bay, preferentially avoiding the substantially decreased σ_f area that continued to envelope the central Bay owing to the 1838 and 1868 earthquakes. Choosing a nucleation point of the 1906 earthquake near the Golden Gate [*Wald et al.*, 1993], as seen in the 1906⁻ snapshot (Figure 9i), the 1906 earthquake nucleated in a point of elevated σ_f because the Golden Gate area was likely at the northern tip of the 1838 rupture. By that time, much of the 1838 stress shadow in the peninsula had been eroded, but more importantly the northern San Andreas fault (north of the Golden Gate) was under very high stress because of the lack of stress release in the north Bay during the preceding decades, compounded by postseismic relaxation effects from the 1838 and 1892 earthquakes which loaded the northern San Andreas fault even more (the 1838 earthquake through enhanced τ , the 1892 earthquakes through enhanced σ_n , i.e., unclamping of the San Andreas fault). The primary feature of the actual slip distribution of

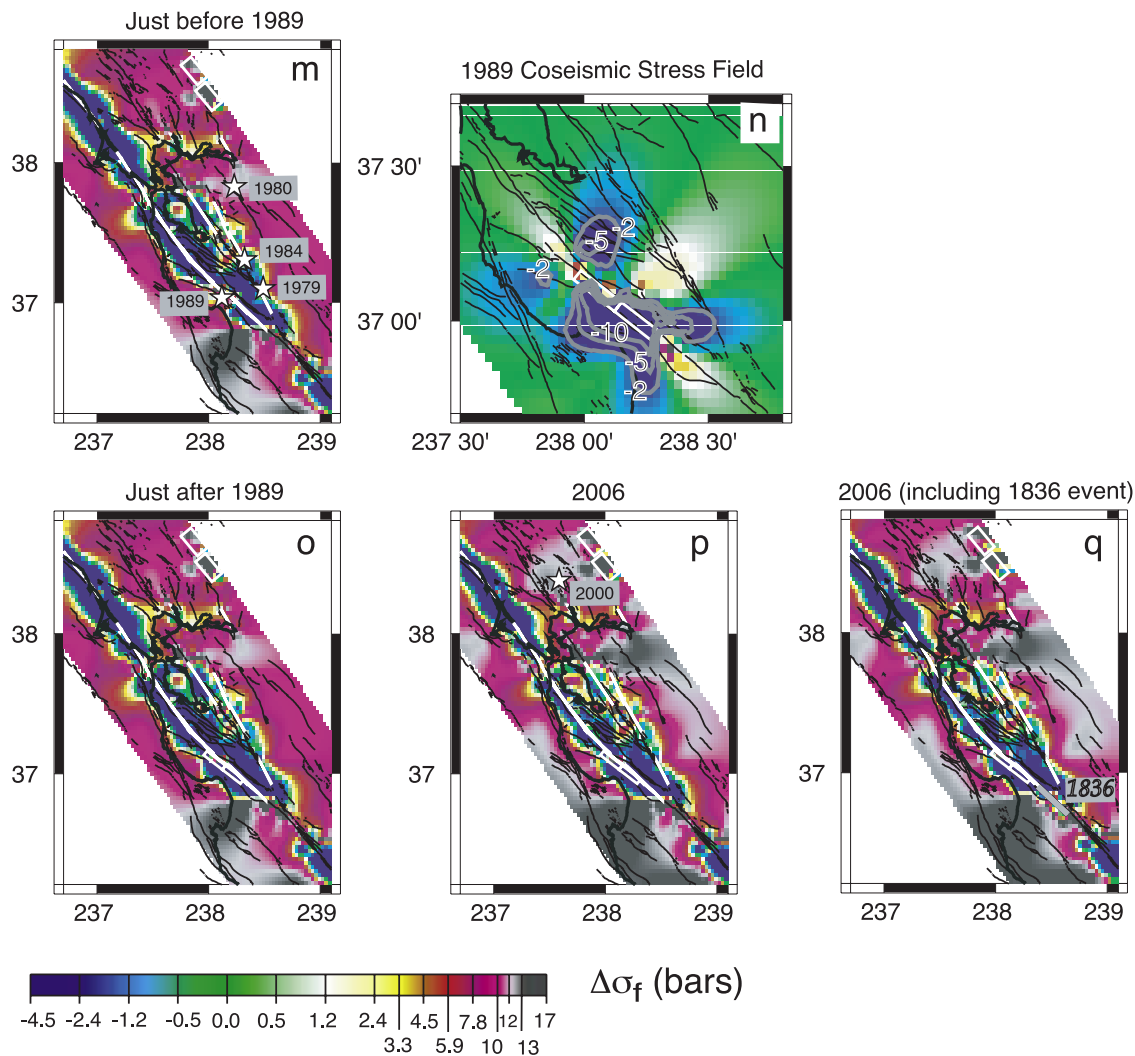


Figure 9. (continued)

the 1906 earthquake (Figure 10) is the much larger slip north of the Golden Gate than to its south. From the 1906⁻ snapshot (Figure 9h), this feature is clearly correlated with the σ_f pattern predicted just before the 1906 earthquake.

[23] The occurrence of the 1906 San Francisco earthquake enveloped practically the entire region in a large stress shadow. As seen in the 1906⁺ and subsequent snapshots (Figures 9i–9l), this shadow persisted for several decades, and seismicity rates plunged for about 70 years after the earthquake. Beginning around 1980 (Figure 9m) the SFBR began to emerge from the 1906 stress shadow. The northern part of the East Bay, the north Bay sufficiently east of the San Andreas fault, and the southern Santa Cruz Mountains regions emerged most prominently because their associated stress levels were already elevated several bars above the regional average even just after the 1906 earthquake (Figure 9i). It is noteworthy that this pattern was largely inherited from the pre-1906 rupture history, i.e., many of the features of the stress pattern seen in the 1906⁻ snapshot (Figure 9i) persist up to the present time. In the central part of the north Bay in the vicinity of the 2000 Yountville $M = 5.2$ earthquake, σ_f increased more than surrounding areas owing to the off-fault effect of the slip

peak of the 1906 earthquake near Tomales Bay (Figure 10). By 1980 it is clear that according to the model, much of the SFBR region had emerged from the stress shadow, and the increase in seismicity rate in the 1980s is consistent with that result.

4. Discussion

[24] A useful way to summarize the stress evolution in the SFBR since 1838 is to track the average stress of the region through time, enabling us to characterize potential source regions in terms of those areas which had stress levels above or below the regional average. For three possible values of the effective coefficient of friction, Figure 11 shows the average σ_f in a region that encompasses the whole PBZ (solid line in each subplot) or the central half of the PBZ (dashed line in each subplot). The second measure is generally a few bars below the first measure because the central half of the PBZ samples mostly the active faulting areas and hence more of those areas strongly affected by the stress shadows from the 1838, 1868, and 1906 events. Figure 11 includes model σ_f at the times and locations of all 22 potentially triggered earthquakes. We find that almost

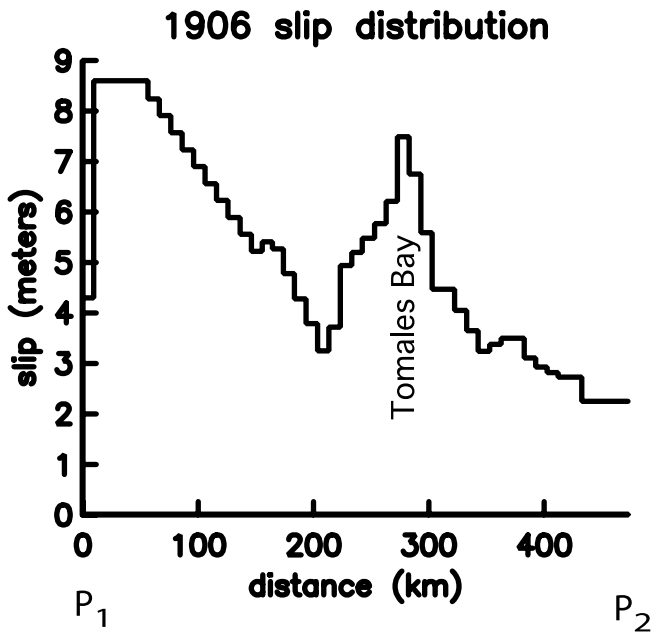


Figure 10. Slip distribution of the 1906 San Francisco earthquake [Thatcher et al., 1997]. P_1 and P_2 correspond to the northern and southern San Andreas fault endpoints indicated in Figure 2.

all potentially triggered earthquakes occurred in regions elevated 5 to 10 bars above the regional average. Since any earthquake occurring within the part of the PBZ occupied by faults has an equal chance of lying above or below the dashed line, this indicates a systematic pattern of historical earthquake occurrence which is extremely unlikely to have occurred by chance. (The probability of 19 of 22 events lying in a positive σ_f region by chance is 0.04%.) This pattern is produced regardless of the value of the effective coefficient of friction. This confirms the marked tendency displayed in the stress evolution plots (Figures 9a–9q): historical and contemporary SFBR earthquakes are systematically located away from shadows zones. This tendency is manifested equally for both pre-1906 and post-1906 earthquakes. It suggests that the constructive and destructive interference patterns created by the melange of 19th century earthquakes and the 1906 earthquake are to first order captured by our physical model. It further suggests that our model carries predictive power for where moderate to large earthquakes are likely to occur in the future. An absolute stress level of zero in Figure 11 is a meaningful reference point: it is the absolute stress level of the inner PBZ (dashed line in Figure 11a) just before the 1906 earthquake. Given that the SFBR was very active in the 40 years prior to 1906 (seven $M \geq 6.2$ events between 1868 and 1906), when σ_f was at or below this level, a recent return to this level would imply a return to conditions when $M \geq 6.2$ earthquakes were occurring relatively frequently. If correct, our model predicts that the SFBR emerged from the 1906 stress shadow in 1980, and since then average stress levels are comparable with those that prevailed in the few decades prior to 1906. This rationalizes Bakun’s [1999] observation that the post-1977 moment release rate is roughly equal to the moment release

rate during the 56 years preceding the 1906 earthquake. The recurrence time for the 1906 earthquake is thought to be about 250 years. We note that with a slip accumulation rate of about 30 mm/yr, the 80 years time needed to erode the

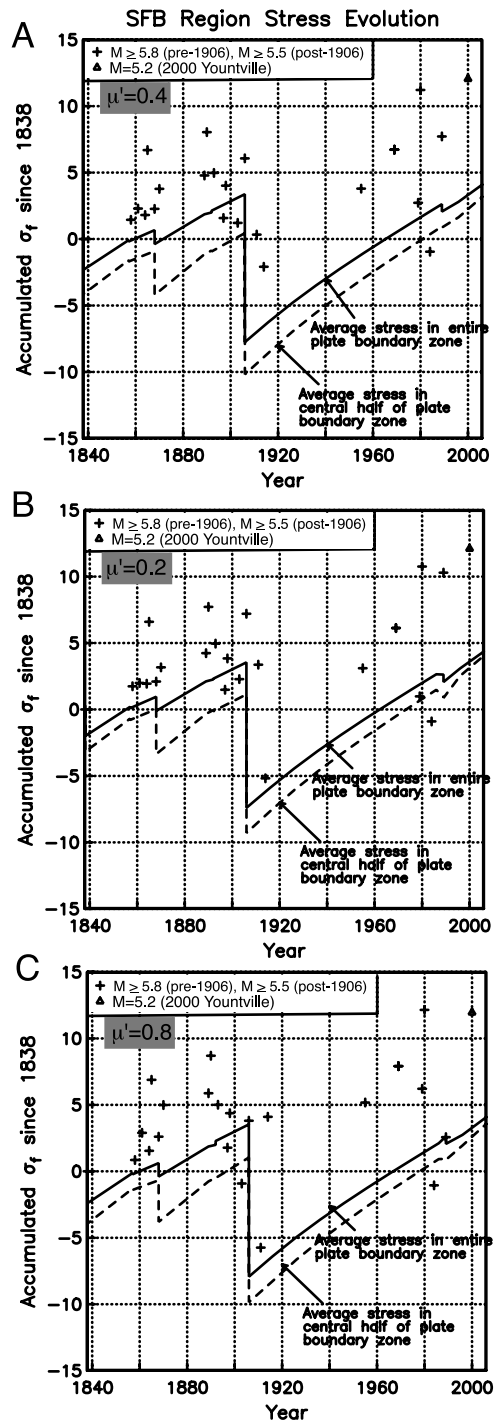


Figure 11. Regionally averaged σ_f within an area encompassing the entire PBZ (region ABCD in Figure 2), shown by the solid line, or within the central half of the PBZ (region A'B'C'D' in Figure 2), shown by the dashed line. The crosses represent model σ_f at the times and locations of the 22 potentially triggered earthquakes shown in Figure 8. Figures 11a, 11b, and 11c show results for the indicated values of effective coefficient of friction.

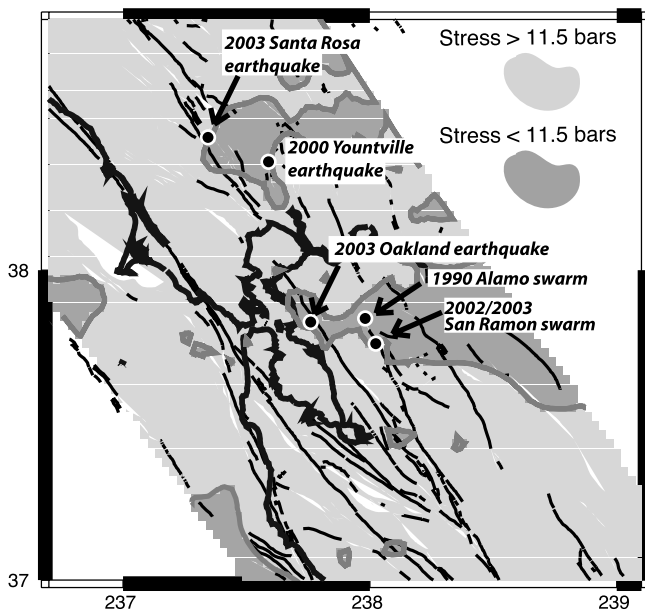


Figure 12. Areas of greatest stress concentration in 2003 as predicted by the model. Locations of several moderate earthquakes are superimposed: the 3 September 2000 Yountville $M = 5.2$ earthquake, the 25 May 2003 Santa Rosa $M = 4.3$ earthquake, the 5 September 2003 $M = 4.2$ Oakland earthquake, the 1990 Alamo swarm (several earthquakes of magnitude from 3.0 to 4.5), and the 2002/2003 San Ramon swarm (several earthquakes of magnitude from 3.0 to 4.2).

shadow is consistent with the average ~ 3 m slip in 1906 south of the Golden Gate [Thatcher *et al.*, 1997].

[25] The earthquake history assumed here is based on fragmentary information for most 19th century events. We have assumed that the northern extent of the 1838 rupture is just south of the Golden Gate. However, it is possible that the 1838 rupture extended only slightly farther north than Woodside, where likely 1838 slip is documented [Toppozada and Borchardt, 1998; Bakun, 1999]. The precise location of the northern termination carries implications for triggering of the 1868 and 1906 earthquakes as well as the long-lived stress pattern in the East Bay. A northern 1838 termination as far south as Woodside would reduce σ_f near the Golden Gate at the time of the 1906 earthquake, but with postseismic relaxation effects the Golden Gate area (where the 1906 rupture is thought to have nucleated) would still be perturbed several bars positive relative to surrounding regions. A northern termination located farther south than we have assumed would also reduce the short-term and long-term σ_f on the central Hayward and northern Calaveras faults and enhance the σ_f on the southern Hayward and central Calaveras faults. This is because the σ_f pattern in the East Bay imparted by the 1838 earthquake arises primarily from the normal stress change, the position of which is controlled by the 1838 fault endpoints. In the short term, higher σ_f on the southern Hayward fault in the years following 1838 is still consistent with triggering of the 1868 earthquake. In the long-term, higher σ_f on the central Calaveras fault imparted by the 1838

earthquake, projected up to the present time, would complement relatively high σ_f on the northern Calaveras fault imparted by the 1868 earthquake. In this case, the positive correlations of the σ_f pattern with the post-1906 history of earthquake occurrence in the East Bay (Figure 11) remain strong.

[26] It is possible to reverse the reasoning pattern if we seek to understand the geometry of historic ruptures. The northern terminations of both the 1838 and 1868 earthquakes are uncertain, but their respective locations combined have a profound effect on resulting East Bay stress patterns throughout time. If positive stress correlations in the record of East Bay earthquakes are considered indicative of a plausible stress evolution model, then the earthquake pattern itself may potentially provide a useful guide to the fault endpoints of important, yet poorly constrained historic ruptures. From this point of view, the positive σ_f correlations that are consistently obtained for the triggered East Bay events (Figures 9a–9q, 11, and 12) suggest that the chosen northern terminations of the 1838 and 1868 events are consistent with our explanation of subsequent seismicity.

[27] Additional shortcomings of our modeling are that we have neglected the effects of large earthquakes that occurred in 1836 and 1865. Different possible scenarios for the locations and fault geometries of these earthquakes are presented by Bakun [1998]. A location of the $M \sim 6.5$ 1865 earthquake on the SAF (scenario B of Bakun [1998]), possibly coinciding with the Loma Prieta rupture zone, cannot be ruled out, and it would be consistent with triggering from the 1838 earthquake (Figure 9d). Triangulation data hint at scenario A of Bakun [1998] in which the 1865 earthquake occurred near the Berrocal fault zone. In either case, likely thrust faulting associated with the 1865 event would have resulted in short-term and long-term stressing of the southern Hayward and central Calaveras faults. In particular, a location of the 1865 event on the Berrocal fault would have strongly increased σ_f on the southern Hayward fault (by a few bars) at the time of the 1868 earthquake, and correspondingly larger σ_f would consequently persist up to the present time. The $M \sim 6.5$ 1836 earthquake may have occurred on either the SAF (scenario B of Bakun, 1998) or Sargent fault (scenario A of Bakun [1998]) near Monterey Bay. In either case, inclusion of the regional stress perturbations resulting from a 1836 source would reduce σ_f on faults southwest of the SAF. This is the location of a predicted local stress maximum (e.g., 2006 snapshot in Figure 9p), which arises from the fact that strain accumulation within the PBZ (distributed 38 mm/yr slip rate) is not completely relieved by the creep along the NW creeping segment of the SAF and the Calaveras fault, which totals only 24 mm/yr in our model (Figure 6). Inclusion of a 1836 event near Monterey Bay would help reduce the buildup of stress that cannot be achieved through fault creep alone. To test this idea we implemented an 1836 source similar to scenario B of Bakun [1998], but with the fault shifted about 10 km to the southeast to remove overlap of it with the 1890 earthquake. The 2006 stress pattern calculated with the additional 1836 source effects (Figure 9q) yields somewhat reduced stress southwest of Monterey Bay, but most of the stress buildup remains. We suggest that either this local stress maximum is real, or additional dislocations sources in the past have

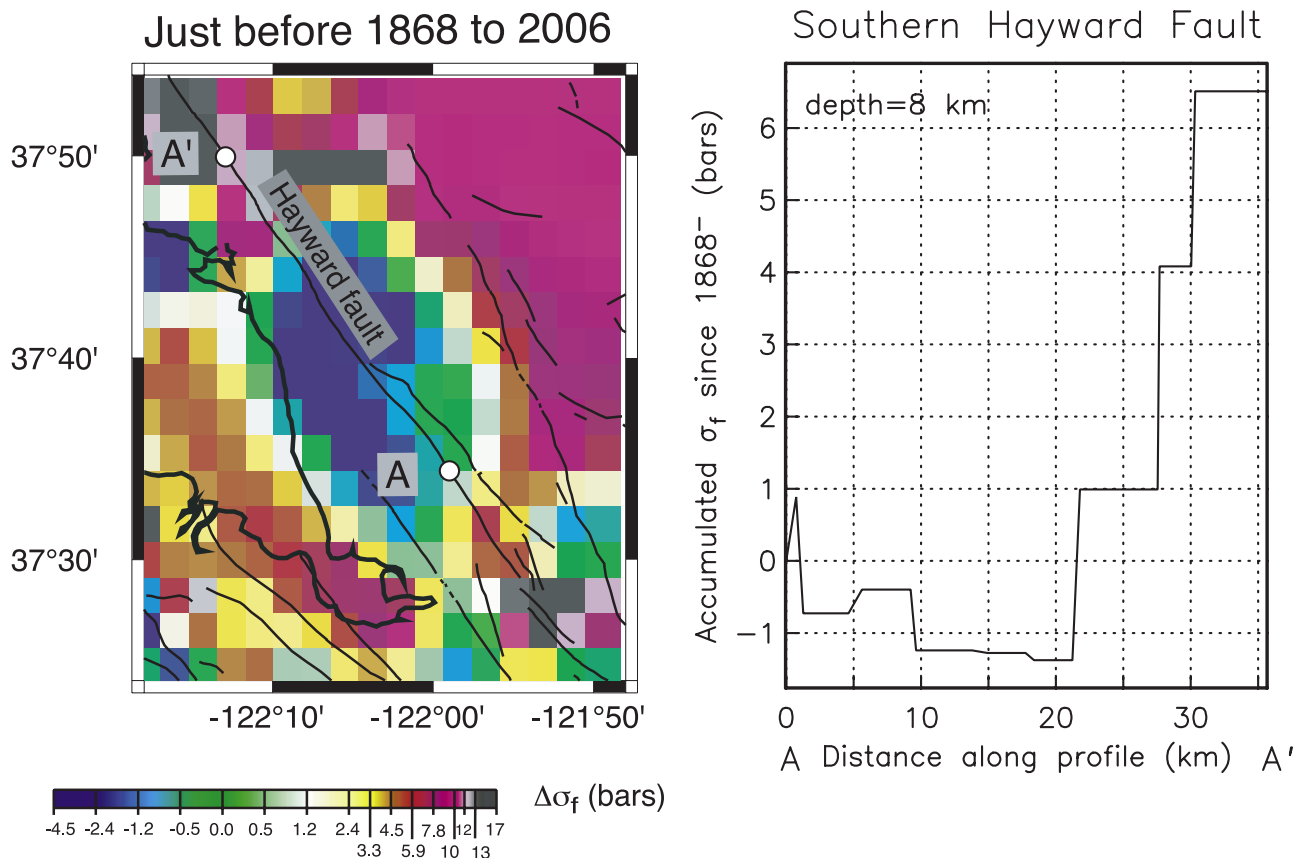


Figure 13. Predicted σ_f in 2006 accumulated since just before the 1868 Hayward fault earthquake.

helped dissipate it, such as accelerated creep along the local SAF or numerous slow earthquakes which are known to have recently affected the region [Linde *et al.*, 1996].

[28] We present a simplified view of present-day stress in Figure 12, where we delineate which regions are above and below a certain σ_f value. The high- σ_f regions are considered to represent areas of present-day stress concentration. Although no large ($M \geq 5.5$) events have occurred in the region since the 1989 Loma Prieta earthquake, the locations of several recent moderate earthquakes are consistent with predicted areas of stress concentration. It is noteworthy that with the exception of the 5 September 2003 Oakland earthquake, all of the recent events have occurred on essentially locked segments of the Calaveras fault or north Bay faults (Napa fault, Rodgers Creek fault).

[29] *Topozada et al.* [2002] have noted that the SFBR has been almost entirely devoid of $M > \sim 5$ earthquakes since the 1989 Loma Prieta earthquake. Although the region is on average as highly stressed as it was during the decades preceding 1906, the distribution of stress is different, presently being more concentrated in the East Bay rather than the west Bay (Peninsula) as it was before 1906. The effect of the 1989 earthquake was to reduce σ_f not only within the 1989 fault zone but also on parts of the Berrocal, southern Hayward, and southern Calaveras faults (Figure 9n). These are among the few regions in the southern SFBR that were highly stressed prior to 1989, so it is conceivable that the coseismic stress change of the 1989 earthquake particularly affected those areas that were otherwise most likely to rupture. The only significant areas of

positive σ_f imparted by the 1989 earthquake are on the Calaveras fault near Morgan Hill, where stress levels had already been reduced by the 1984 Morgan Hill earthquake, and the San Andreas fault near San Juan Bautista. This part of the San Andreas fault, which creeps at about 12 mm/yr, has been the most seismically active part of the SFBR, e.g., the 12 August 1999 San Juan Bautista $M = 5.1$ earthquake [Uhrhammer *et al.*, 1999]. Thus the near absence of $M > 5$ regional earthquakes since 1989 may to a large extent reflect the temporary reduction of stress on active parts of the southern Hayward and Calaveras faults.

[30] Stress heterogeneity must have existed in the region prior to 1838, and this of course complicates any interpretation of even relative stress levels in terms of seismic potential. For example, the southern Hayward fault which ruptured with a large earthquake in 1868 was obviously only 30 years from releasing a large amount of built-up stress in 1838. Since this fault ruptures fairly regularly with a recurrence time of about 130 years [Lienkaemper *et al.*, 2002], one should expect its present stress level (we are presently 135 years since the last rupture) to be comparable to the stress levels which existed in 1868. Figure 13 suggests that this is the case: about one third of the southern Hayward fault is presently ~ 1 –6 bars more greatly stressed than it was just prior to the 1868 earthquake, and the remainder is only ~ 1.5 bars less stressed, and even these areas would be predicted to attain pre-1868 stress levels in an additional 15 years. Thus the stress evolution model is consistent with the known recurrence interval of the Hayward fault but can only shed light on its stress state relative

to that which existed just prior to 1838. In principle, one could use the history of past rupture on the Hayward, Rodgers Creek, and other faults to calibrate the initial stress state that existed at the 1838 initiation time, assuming that each last previous large rupture on these distinct faults occurred at similar absolute stress levels, although this cannot be known with certainty. Some guidance is provided by the fact that no $M \geq 7$ earthquakes occurred in the SFBR between 1776 and 1836 [Ellsworth, 1990]. Most of the region may have been in a half-century-long stress shadow during this time because of large events inferred to have occurred on the Rodgers Creek, North Hayward, South Hayward, and San Andreas faults from ~ 1650 to ~ 1770 from paleoseismological evidence (D. Schwartz, personal communication, 2003). In addition, assuming that numerous small and moderate earthquakes occurred from 1776 to 1838, it is conceivable that these smaller shocks helped homogenize the stress field prior to about 1838. Such a possibility is suggested by theoretical considerations in which a region that is characterized by intermittent criticality will exhibit an increasingly white wave number spectrum (with respect to stress) with time into a large earthquake cycle [Ben-Zion et al., 2003]. If true, then the stress field just prior to 1838 would have exhibited variations about equally at all spatial scales.

[31] Earthquake probabilities in the SFBR have been estimated using a suite of models [Working Group on California Earthquake Probabilities, 2003], in which integrated information on fault slip histories were interpreted using an empirical model [Reasenberget al., 2003], Poissonian and renewal models. In the latter case, time-dependent fault interaction effects from the 1906 earthquake were incorporated through time advances or delays associated with the coseismic stress step. A more comprehensive treatment of time-dependent stressing effects was not attempted because a suitable physical model was not available. We expect that the regional time-dependent stressing history estimated in this paper will be useful for revising regional earthquake probabilities and allowing more comprehensive time-dependent forecasts in the future.

5. Conclusions

[32] Stress evolution in the SFBR is investigated using a simple physical model derived from recent GPS measurements. The main contributing processes to regional strain accumulation are regarded as background Pacific-SNGV loading through horizontally transmitted shear, viscoelastic relaxation of the lower crust and upper mantle following major earthquakes, and steady creep along certain faults. We assume that the SFBR is well characterized as a ~ 135 km wide plate boundary zone with a relatively thin lithosphere surrounded by the relatively thick lithosphere of the Pacific and SNGV plates. Assuming uniform viscoelastic properties of the plate boundary zone, we use a superposition of special solutions to the equations of quasi-static equilibrium, enabling us to describe the evolution of quasi-static displacement with nearly constant Pacific-SNGV relative velocity along the plate boundary zone edges.

[33] This model is evaluated forward in time by integrating the time-dependent stressing rates and the coseismic deformation fields from the major historical earthquakes.

The resulting time-dependent Coulomb failure stress patterns (accumulated σ_f since 1838) are compared with the history of moderate to large earthquakes. We find that nearly all earthquakes occur in areas of stress elevated about 5–10 bars above the regional average. The SFBR is predicted to have emerged from the 1906 stress shadow in about 1980, which is consistent with the acceleration in regional seismicity at about that time following a long period of relative inactivity after the 1906 earthquake. Taken at face value, our physical model predicts that, on average, the SFBR is under the same stress levels that existed during the few decades prior to the 1906 earthquake. Although the detailed distribution of σ_f from 1850 to 1906 compared with post-1980 σ_f is different, we suggest that the SFBR seismicity rates should continue at post-1977 levels (1.36×10^{18} N m/yr) or greater, and the spatial distribution of present-day σ_f is a useful guide to the locations of future moderate to large SFBR earthquakes.

[34] **Acknowledgments.** This paper benefitted from internal reviews by Paul Reasenberget Bob Simpson and discussions with Roland Bürgmann, David Schwartz, Tom Parson, and Mary-Lou Zoback. We are grateful to the Associate Editor, Kaj M. Johnson, and an anonymous reviewer for their constructive comments.

References

- Argus, D. F., and R. G. Gordon (2001), Present tectonic motion across the Coast Ranges and San Andreas fault system in central California, *Geol. Soc. Am. Bull.*, *113*, 1580–1592.
- Bakun, W. H. (1998), Scenarios for historic San Francisco Bay region earthquakes, *U.S. Geol. Surv. Open File Rep.*, *98-785*, 14 pp.
- Bakun, W. H. (1999), Seismic activity of the San Francisco Bay region, *Bull. Seismol. Soc. Am.*, *89*, 764–784.
- Ben-Zion, Y., M. Eneva, and Y. Liu (2003), Large earthquake cycles and intermittent criticality on heterogeneous faults due to evolving stress and seismicity, *J. Geophys. Res.*, *108*(B6), 2307, doi:10.1029/2002JB002121.
- Ellsworth, W. L. (1990), Earthquake history, 1769–1989, in *The San Andreas Fault System, California*, edited by R. E. Wallace, *U.S. Geol. Surv. Prof. Pap.*, *1515*, 153–188.
- Fumal, T. E., T. E. Dawson, R. Flowers, J. C. Hamilton, and L. Samrad (2003), Photomosaics and logs of trenches on the San Andreas fault at Mill Canyon near Watsonville, California, *U.S. Geol. Surv. Open File Rep.*, *03-469*.
- Galehouse, J. S. (1997), Effect of the Loma Prieta earthquake on fault creep rates in the San Francisco Bay region, in *The Loma Prieta, California, Earthquake of October 17, 1989: Aftershocks and Postseismic Effects*, edited by P. A. Reasenberget al., *U.S. Geol. Surv. Prof. Pap.*, *1550D*, 193–207.
- Harris, R. A., and R. W. Simpson (1998), Suppression of large earthquakes by stress shadows: A comparison of Coulomb and rate-and-state failure, *J. Geophys. Res.*, *103*, 24,439–24,451.
- Hole, J. A., T. M. Brocher, S. L. Klemperer, T. Parsons, H. M. Benz, and K. P. Furlong (2000), Three-dimensional seismic velocity structure of the San Francisco Bay area, *J. Geophys. Res.*, *105*, 13,859–13,874.
- Jaume, S. C., and L. R. Sykes (1996), Evolution of moderate seismicity in the San Francisco Bay region, 1850 to 1993: Seismicity changes related to the occurrence of large and great earthquakes, *J. Geophys. Res.*, *101*, 765–789.
- Kelson, K. I., W. R. Lettis, and M. Lisowski (1992), Distribution of geologic slip and creep along faults in the San Francisco Bay region, in *Proceedings of the Second Conference on Earthquake Hazards in the Eastern San Francisco Bay Area*, edited by G. Borchardt et al., *Spec. Publ. Calif. Div. Mines Geol.*, *113*, 31–38.
- Kenner, S. J., and P. Segall (1999), Time dependence of the stress shadowing effect and its relation to the structure of the lower crust, *Geology*, *27*, 119–122.
- King, G. C., R. S. Stein, and J. Lin (1994), Static stress changes and the triggering of earthquakes, *Bull. Seismol. Soc. Am.*, *84*, 935–953.
- Lienkaemper, J. J., J. S. Galehouse, and R. W. Simpson (1997), Creep response of the Hayward fault to stress changes caused by the Loma Prieta earthquake, *Science*, *276*, 2014–2016.
- Lienkaemper, J. J., T. E. Dawson, S. F. Personius, G. G. Seitz, L. M. Reidy, and D. P. Schwartz (2002), A record of large earthquakes on the southern Hayward fault for the past 500 years, *Bull. Seismol. Soc. Am.*, *92*, 2637–2658.

- Linde, A. T., M. T. Gladwin, M. J. S. Johnston, R. L. Gwyther, and R. G. Bilham (1996), A slow earthquake sequence near San Juan Bautista, California in December 1992, *Nature*, *383*, 65–69.
- Marshall, G. A., R. S. Stein, and W. Thatcher (1991), Faulting geometry and slip from co-seismic elevation changes: The October 17, 1989 Loma Prieta earthquake, *Bull. Seismol. Soc. Am.*, *81*, 1660–1693.
- Murray, M. H., and P. Segall (2001), Modeling broadscale deformation in northern California and Nevada from plate motions and elastic strain accumulation, *Geophys. Res. Lett.*, *28*, 4315–4318.
- O'Connell, D. R. H., J. R. Unruh, and L. V. Block (2001), Source characterization and ground motion modeling of the 1892 Vacaville-Winters earthquake sequence, California, *Bull. Seismol. Soc. Am.*, *91*, 1471–1497.
- Oppenheimer, D. H., W. H. Bakun, and A. G. Lindh (1990), Slip partitioning of the Calaveras fault, California, and prospects for future earthquakes, *J. Geophys. Res.*, *95*, 8483–8498.
- Parsons, T. (2002), Post-1906 stress recovery of the San Andreas fault system calculated from three-dimensional finite element analysis, *J. Geophys. Res.*, *107*(B8), 2162, doi:10.1029/2001JB001051.
- Parsons, T., R. S. Stein, R. W. Simpson, and P. A. Reasenberg (1999), Stress sensitivity of fault seismicity: A comparison between limited-offset oblique and major strike-slip faults, *J. Geophys. Res.*, *104*, 20,183–20,202.
- Pollitz, F. F. (1996), Coseismic deformation from earthquake faulting on a layered spherical Earth, *Geophys. J. Int.*, *125*, 1–14.
- Pollitz, F. F. (1997), Gravitational-viscoelastic postseismic relaxation on a layered spherical Earth, *J. Geophys. Res.*, *102*, 17,921–17,941.
- Pollitz, F. F. (2001), Viscoelastic shear zone model of a strike-slip earthquake cycle, *J. Geophys. Res.*, *106*, 26,541–26,560.
- Pollitz, F. F., and M. Nyst (2004), A physical model for strain accumulation in the San Francisco Bay region, *Geophys. J. Int.*, in press.
- Pollitz, F. F., R. Bürgmann, and P. Segall (1998), Joint estimation of after-slip rate and viscoelastic relaxation following the 1989 Loma Prieta earthquake, *J. Geophys. Res.*, *103*, 26,975–26,992.
- Prescott, W. H., J. C. Savage, J. L. Svarc, and D. Manaker (2001), Deformation across the Pacific–North America plate boundary near San Francisco, California, *J. Geophys. Res.*, *106*, 6673–6682.
- Reasenberg, P. A., and R. W. Simpson (1992), Response of regional seismicity to the static stress change produced by the Loma Prieta earthquake, *Science*, *255*, 1687–1690.
- Reasenberg, P. A., T. C. Hanks, and W. H. Bakun (2003), An empirical model for earthquake probabilities in the San Francisco Bay region, California, *Bull. Seismol. Soc. Am.*, *93*, 1–13.
- Rymer, M. J., M. Lisowski, and R. O. Burford (1984), Structural explanation for low creep rates on the San Andreas fault near Monarch Peak, central California, *Bull. Seismol. Soc. Am.*, *74*, 925–931.
- Savage, J. C., and M. Lisowski (1993), Inferred depth of creep on the Hayward fault, central California, *J. Geophys. Res.*, *98*, 787–793.
- Savage, J. C., and W. H. Prescott (1978), Asthenospheric readjustment and the earthquake cycle, *J. Geophys. Res.*, *83*, 3369–3376.
- Savage, J. C., R. W. Simpson, and M. H. Murray (1998), Strain accumulation rates in the San Francisco Bay area, 1972–1998, *J. Geophys. Res.*, *103*, 18,039–18,051.
- Savage, J. C., J. L. Svarc, and W. H. Prescott (1999), Geodetic estimates of fault slip rates in the San Francisco Bay area, *J. Geophys. Res.*, *104*, 4995–5002.
- Schwartz, D. P., D. Pantosti, K. Okumura, T. J. Powers, and J. Hamilton (1998), Paleoseismic investigations in the Santa Cruz mountains, California: Implications for recurrence of large-magnitude earthquakes on the San Andreas fault, *J. Geophys. Res.*, *103*, 17,985–18,001.
- Sieh, K. (1978), Slip along the San Andreas fault associated with the great 1857 earthquake, *Bull. Seismol. Soc. Am.*, *68*, 1421–1428.
- Simpson, R. W., and P. A. Reasenberg (1994), Earthquake-induced static stress changes on central California faults, in *The Loma Prieta, California, Earthquake of October 17, 1989—Tectonic Processes and Models*, edited by R. W. Simpson, *U.S. Geol. Surv. Prof. Pap.*, *1550F*, 55–89.
- Simpson, R. W., J. J. Lienkaemper, and J. S. Galehouse (2001), Variations in creep rate along the Hayward fault, California interpreted as changes in depth of creep, *Geophys. Res. Lett.*, *28*, 2269–2272.
- Stein, R. S. (1999), The role of stress transfer in earthquake occurrence, *Nature*, *402*, 605–609.
- Thatcher, W. (1983), Nonlinear strain buildup and the earthquake cycle on the San Andreas fault, *J. Geophys. Res.*, *88*, 5893–5902.
- Thatcher, W., G. Marshall, and M. Lisowski (1997), Resolution of fault slip along the 470-km-long rupture of the great 1906 San Francisco earthquake and its implications, *J. Geophys. Res.*, *102*, 5353–5367.
- Topozada, T. R., and G. Borchart (1998), Re-evaluation of the 1836 “Hayward fault” and the 1838 San Andreas earthquakes, *Bull. Seismol. Soc. Am.*, *88*, 140–159.
- Topozada, T. R., and D. Branum (2002), California $M \geq 5$ earthquakes, history, and areas damaged, in *International Handbook of Earthquake and Engineering Seismology*, edited by W. H. Lee, H. Kanamori, and P. Jennings, chapter 48.1, Int. Assoc. of Seismol. and Phys. of the Earth's Inter., Boulder, Colo.
- Topozada, T. R., D. M. Branum, M. S. Reichle, and C. L. Hallstrom (2002), San Andreas fault zone, California: $M \geq 5.5$ earthquake history, *Bull. Seismol. Soc. Am.*, *92*, 2555–2601.
- Tuttle, M. P., and L. R. Sykes (1992), Re-evaluation of several large historic earthquakes in the vicinity of the Loma Prieta and Peninsular segments of the San Andreas fault, California, *Bull. Seismol. Soc. Am.*, *82*, 1802–1820.
- Uhrhammer, R., L. S. Gee, M. Murray, D. Dreger, and B. Romanowicz (1999), The M_w 5.1 San Juan Bautista, California earthquake of 12 August 1998, *Bull. Seismol. Soc. Am.*, *70*, 10–18.
- Wald, D. J., H. Kanamori, D. V. Helmlinger, and T. H. Heaton (1993), Source study of the 1906 San Francisco earthquake, *Bull. Seismol. Soc. Am.*, *83*, 981–1019.
- Working Group on California Earthquake Probabilities (2003), Earthquake probabilities in the San Francisco Bay region: 2002–2031, *U.S. Geol. Surv. Open File Rep.*, *03-214*. (Available at <http://geopubs.wr.usgs.gov/open-file/of03-214/>)
- Yu, E., and P. Segall (1996), Slip in the 1868 Hayward earthquake from the analysis of historic triangulation data, *J. Geophys. Res.*, *101*, 16,101–16,118.

W. H. Bakun, M. Nyst, and F. Pollitz, U.S. Geological Survey, 345 Middlefield Road, MS 977, Menlo Park, CA 94025, USA. (bakun@usgs.gov; mnyst@usgs.gov; fpollitz@usgs.gov)